International Journal of Image and Data Fusion
Vol. 3, No. 1, March 2012, 71–92

Taylor & Francis
Taylor & Francis Group

Fusion of D-InSAR and sub-pixel image correlation measurements for coseismic displacement field estimation: Application to the Kashmir earthquake (2005)

Yajing Yan[ab]*, Emmanuel Trouvé[a], Virginie Pinel[b], Gilles Mauris[a], Erwan Pathier[c] and Sylvie Galichet[a]

[a]*Laboratoire d'Informatique, Systèmes, Traitement de l'Information et de la Connaissance, Université de Savoie, Polytech Annecy-Chambéry, BP 80439, Annecy-le-Vieux Cedex F-74944, France;* [b]*ISTerre, IRD R219, CNRS, Université de Savoie, Campus Scientifique, Le Bourget du Lac Cedex 73376, France;* [c]*Université de Joseph Fourier, BP 53, 38041, Grenoble, France*

(*Received 6 December 2010; final version received 21 March 2011*)

In geophysics, the uncertainty associated with model parameters or displacement measurements plays a crucial role in the understanding of geophysical phenomenon. An emerging way to reduce the geodetic parameter uncertainty is to combine a large number of data provided by SAR images. However, the measurements by radar imagery are subject to both random and epistemic uncertainties. Probability theory is known as the appropriate theory for random uncertainty, but questionable for epistemic uncertainty. Fuzzy theory is more adapted to epistemic uncertainty. Moreover, in a context of random and epistemic uncertainties, the conventional joint inversion in the least squares sense cannot be considered any more as the best scheme to reduce uncertainty. Therefore, in this article, in addition to joint inversion, two other fusion schemes, pre-fusion and post-fusion, are proposed. We consider here the conventional approach and an original fuzzy approach for handling random and epistemic uncertainties of D-InSAR and sub-pixel image correlation measurements. Joint inversion and pre-fusion are then applied to the measurement of displacement field due to the 2005 Kashmir earthquake by fusion of these data. The behaviours of these two fusion schemes versus uncertainty reduction are highlighted through comparisons of results.

Keywords: measurement uncertainty; fuzzy theory; fusion scheme; ground displacement; SAR image

1. Introduction

Geodetic data, such as satellite images (radar and optic), is an important remote sensing source of information for displacement measurement with great accuracy over large area. So far, with the increasing number of operational sensors, large volumes of SAR images acquired in different modes, ascending and descending passes at various incident angles and frequencies, are available. Moreover, the launching of the future satellite generation Sentinel in the coming years, will provide a large quantity of free SAR data (Attema 2005).

*Corresponding author. Email: yajing.yan@univ-savoie.fr

ISSN 1947–9832 print/ISSN 1947–9824 online

http://dx.doi.org/10.1080/19479832.2011.577563
http://www.tandfonline.com

Consequently, using a large number of geodetic measurements in order to quantify the displacement precisely and better constrain geophysical modelling is becoming more frequent in geophysics. In (Pedersen *et al.* 2003, Schmidt *et al.* 2005, Sudhaus and Jónsson 2009), the authors assimilated SAR data and GPS data to estimate coseismic slip distributions on faults activated by earthquakes. Grandin *et al.* (2009) combined the measurements from SAR images and optical images to measure the displacement field and to determine the geometry of the dike of the rifting event of Afar (Ethiopia). Lu *et al.* (2010) fused SAR images and optical images to characterise various natural hazards. In this context, one important purpose of geodetic data fusion is to reduce parameter uncertainty by an adequate combination of all the available measurements. In this view, it is important that the retrieval algorithm can also estimate the uncertainty associated with the displacement value, or more generally with the model parameters.

The classical uncertainty concept is based on three classes: gross uncertainty, epistemic uncertainty, and random uncertainty. Gross uncertainty, leading to outliers, has to be avoided or detected by control methods, whereas epistemic uncertainty has to be reduced by correction methods and additional knowledge. The remaining uncertainty is considered as random, and is due to phenomenon variability. In geophysical applications, the measurement uncertainties are, after some pre-processing, considered generally as exclusively random, and thus are represented and propagated in an adequate way by probability tools (Tarantola and Valette 1982, Cervelli *et al.* 2001, Lohman and Simons 2005, Sudhaus and Jónsson 2009). But concerning the measurements by radar (SAR) imagery, the uncertainties arise from several different sources, noise sources of the radar instrument, on the path of radar wave propagation, at the reflecting surface, as well as error sources introduced by data processing (Sudhaus and Jónsson 2009). On one hand, random uncertainty exists due to the decorrelation noise, since there are usually some backscattering property changes on the ground between two subsequent SAR acquisitions. On the other hand, epistemic uncertainties can be induced by atmospheric disturbances depending on the state of atmosphere and the ground surface at the time of the two SAR acquisitions. Also, it can result from the imprecision of orbit auxiliary information, Digital Elevation Model (DEM) errors, as well as from the imperfect corrections during data processing, which deviate the data by a constant or a ramp from the true value. Furthermore, it is worth noting that uncertainties present in radar measurements can be spatially correlated, due to smoothly varying atmospheric signal delays (Doin *et al.* 2009). To model such epistemic uncertainties coming from limited knowledge, the efficiency of probability theory is called into question. Thus fuzzy theory has been investigated in geoscience applications by a few authors (Verhoest *et al.* 2007a,b, Mujumdar and Ghosh 2008, Ross *et al.* 2009, Jacquin 2010). In fact, in geodetic measurements there is a need to select the adequate theory for the representation and propagation of different uncertainties. Therefore, it is worthwhile to study the combination of the most suitable theories since several types of uncertainty occur in geodetic practice. This article is a first contribution to such issues for the measurement of displacement field by fusion of D-InSAR and sub-pixel image correlation measurements with different schemes.

Like in many engineering applications, fusion of information in geodetic applications is often accomplished by a joint inversion of all the available data. For linear model, the least squares adjustment has been widely used because it provides the minimal variance estimation under the assumption of random uncertainties (Tarantola and Valette 1982, Tarantola 2005). Moreover, it leads to simple computations when the measurements are independent. Additionally, when the random variables are Gaussian ones, confidence intervals for the measured parameters can be easily deduced. But in case with both random and epistemic uncertainties, this conventional fusion scheme is debatable. Therefore, in this article we investigate two other fusion schemes: pre-fusion which consists of fusing some data before inversion (in a least squares sense in our case), and post-fusion which consists of performing, firstly several inversions with different subsets of the available data, and then fusing the results of these inversions. In these three fusion schemes, we apply the conventional approach and a fuzzy approach to represent and propagate uncertainties.

This article is organised as follows. In Section 2, joint inversion, pre-fusion and post-fusion schemes are presented. In Section 3, the conventional approach and a fuzzy approach for uncertainty representation and propagation are detailed. The available data in the considered application and their associated uncertainties are described in Section 4. Then, joint inversion and pre-fusion, as well as the proposed uncertainty management approaches are applied to the 3D displacement field measurement at the Earth's surface due to the Kashmir earthquake ($M_w = 7.6, 2005$). The behaviours of these two fusion schemes are highlighted through comparisons of results. Finally, some conclusions are derived and the perspectives are presented.

2. Fusion-inversion schemes

2.1 *Inversion*

In geophysics, modelling allows the explanation of physical processes with the help of an analytically or numerically derived relationship between the observed signal and the characteristics of the source. From the observed signals, the characteristics of the buried source can be inferred once this relationship is determined. This kind of problem is referred to as an inverse problem. Solving an inverse problem is called *inversion* (Tarantola and Valette 1982). If we define the data vector R and the model vector u, the corresponding forward model is written as

$$R = \mathbf{g}(u) \tag{1}$$

where $\mathbf{g}$ is an operator that relates the model vector to the data vector.

When $\mathbf{g}$ consists of linear equations, Equation (1) can be simplified to

$$R = Pu \tag{2}$$

where P corresponds to a $n \times m$ matrix linking the data vector R (dimension: n) and the model vector u (dimension: m).

In general, in the inversion, a misfit function is defined to quantify the discrepancy between observations and model predictions. An inversion algorithm searches for models that minimise the misfit function in the model space which can be bounded by predefined model parameter limits.

In linear inversion, the solutions given by the ordinary least squares (OLS) (Rao 1973, Davidson *et al.* 1993) method and generalised least squares (GLS) (Tarantola 2005, Cornillon and Matzner-Lober 2007) method are shown in Equations (3) and (4), respectively. In most cases, the independence of the used data is assumed in order to facilitate the data processing. With these methods, random uncertainty described by the variance can be optimally reduced depending on the number of data sets used in the inversion.

$$u = (P^T P)^{-1} P^T R \tag{3}$$

$$u = (P^T \Sigma_R^{-1} P)^{-1} P^T \Sigma_R^{-1} R \tag{4}$$

where Σ_R is the variance-covariance matrix of R.

The resolution for a nonlinear problem is usually more complex. There are two main types of algorithms: one is based on the calculation of the derivative (variational approach) and the other is based on Monte Carlo methods (stochastic approach). The methods based on the derivative calculation are commonly used when the relationship between the model and the data is simple. However, when the complexity of this relationship increases, Monte Carlo methods are preferred.

2.2 *Fusion schemes*

Joint inversion (Figure 1(a)), in which all the available data sets are simultaneously combined in the inversion, is the conventional scheme used by most geophysicists. With this scheme, an important point concerning the optimality of the least squares method is that the uncertainty has to be of a random nature, i.e. epistemic uncertainties have to be eliminated beforehand. This is not always possible in a geodetic context, and thus we consider two other fusion schemes: pre-fusion (Figure 1(b)) and post-fusion (Figure 1(c)).

Pre-fusion consists of a fusion step before inversion. This fusion step can be performed for example using the mean value, the median value of a set of data sets or by selecting the best one according to certain criteria, for example, the reliability of data sets or the signal-to-noise ratio. The relevance of this fusion scheme depends on the availability of data sets and the type of uncertainty to be reduced. Afterwards, the refined data sets are input in the inversion.

In post-fusion, first, several inversions are performed with different data subsets. Next, the corresponding inversion results are combined to obtain the final result by a fusion step. Ideally, each data subset used in each inversion should be independent. Therefore, a great number of data sets with a good geographic superposition are required. In addition, post-fusion is interesting for combining results from different sources, such as radar and optical measurements, as well as *in-situ* measurements, because sometimes it can be difficult to mix all these measurements in a joint inversion due to the difficulty in comparing the uncertainties associated with completely different measurements.

3. Uncertainty analysis and management

As mentioned in Section 1, the uncertainty concept is based on three classes: gross uncertainty, epistemic uncertainty, and random uncertainty. Gross uncertainty, leading to outliers, has to be avoided or detected by control methods, and it is not considered in this article. Epistemic uncertainty originates form lack of complete knowledge about the considered phenomenon and observation sources. The variability from one observation to another is generally the result of the random nature of the studied phenomenon and of the noise superposed to the source signals.

Thus, mathematical theories which are appropriate for at least some parts of uncertainty representation and handling have to be considered in a competitive way. Probability theory is the adequate theory for uncertainties corresponding to random

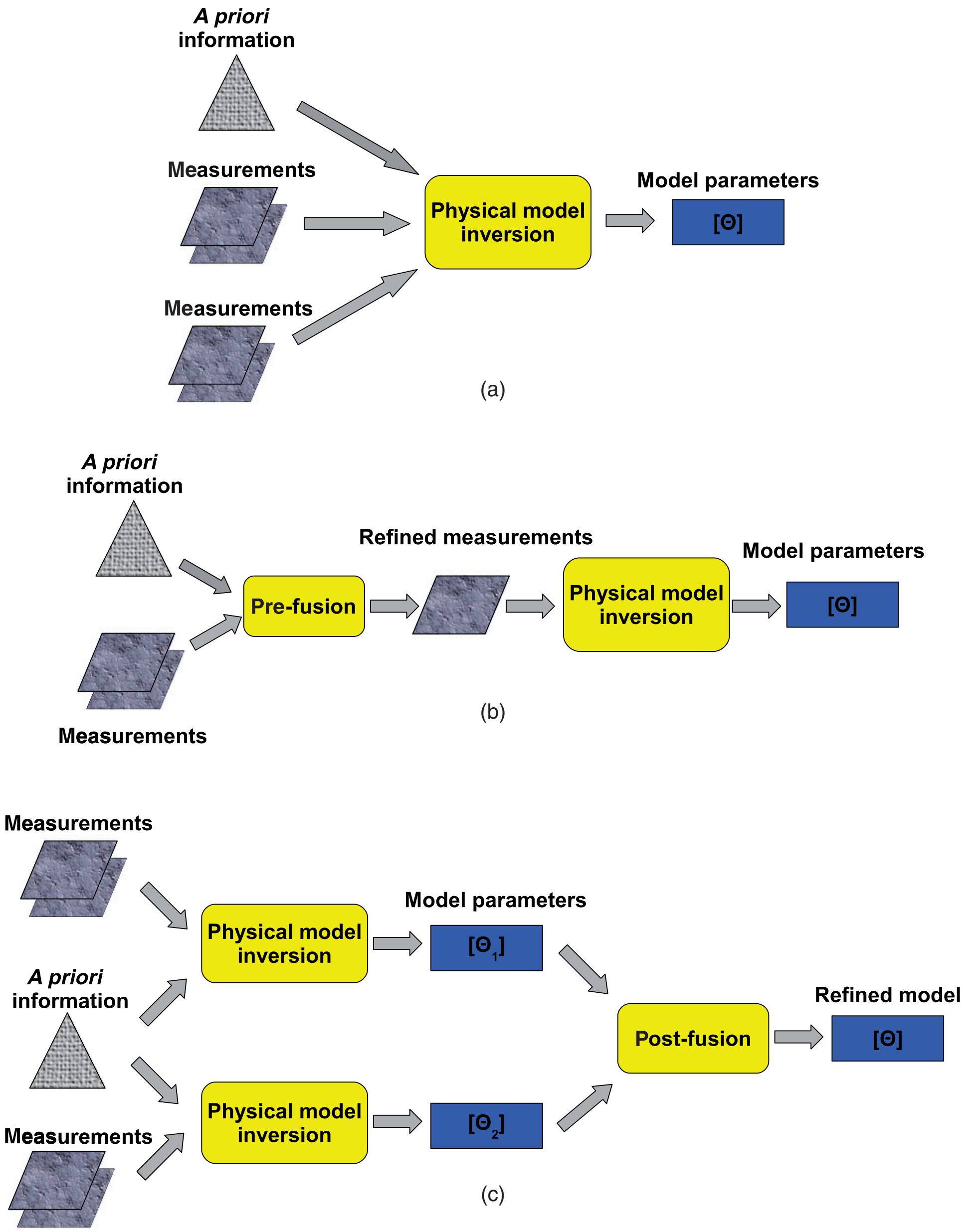

Figure 1. Schematic illustration of fusion schemes. (a) joint inversion, (b) pre-fusion and (c) post-fusion.

variables. In this theory, random variables are described by a probability distribution (often a Gaussian one) or more simply by the first two moments, i.e. the mean and the variance (BIPM *et al.* 2008).

Epistemic uncertainties arising from information incompleteness cannot be represented by one single probability distribution. Dempster–Shafer theory (Shafer 1976) and fuzzy possibility theory (Dubois and Prade 1988) provide relevant representations to deal with epistemic uncertainty. In our context of continuous measurements, the possibility theory is more adapted because it generalises interval analysis and provides a bridge with probability theory by its ability to represent a family of probability distributions (Dubois *et al*. 2004).

In geodetic practice, there are always multiple sources of uncertainties in the considered measurement, which leads to complex characteristics of the associated uncertainties. Therefore, we apply the conventional approach and a fuzzy approach for handling random and epistemic uncertainties.

3.1 *Conventional approach*

The standard reference in uncertainty modelling is the 'Guide to the Expression of Uncertainty in Measurement (GUM)' (BIPM *et al*. 2008) edited by an international consortium of legal and professional organisations. GUM groups the occurring uncertain quantities into 'Type A' and 'Type B'. Uncertainties of 'Type A' are determined with the classical statistical methods, while 'Type B' is subject to other uncertainties like experience and knowledge about an instrument. Both types of uncertainties can have random and epistemic components. In fact, the GUM proposes to treat both uncertainties (random and epistemic) in a stochastic framework, introduces variance to describe uncertainties and treats them with the law of propagation, with the independence generally assumed. Applying this approach to the linear inversion, the uncertainties are propagated as follows.

Let $f_k(x_1, x_2, \ldots, x_n)$ be a set of m functions which are linear combinations of n variables $x_1, x_2, \ldots, x_n$ with combination coefficients $a_{1,k}, a_{2,k}, \ldots, a_{n,k}$, $(k = 1, \ldots, m)$. Thus

$$f_k = \sum_{i=1}^{n} a_{i,k} x_i : f = A^T x \tag{5}$$

If the variance-covariance matrix of x is denoted by Σ_x,

$$\Sigma_x = \begin{pmatrix} \sigma_1^2 & \sigma_{12} & \sigma_{13} & \cdots \\ \sigma_{21} & \sigma_2^2 & \sigma_{23} & \cdots \\ \sigma_{31} & \sigma_{32} & \sigma_3^2 & \cdots \\ \vdots & \vdots & \vdots & \ddots \end{pmatrix} \tag{6}$$

Then, the variance-covariance matrix Σ_f of f is given by

$$\Sigma_{f_{i,j}} = \sum_{k}^{n} \sum_{l}^{n} a_{i,k} \Sigma_{xk,l} a_{l,j} : \Sigma_f = A^T \Sigma_x A \tag{7}$$

This is the most general expression for the propagation of uncertainty from one set of variables onto another. From this, one obtains the variance-covariance matrix of u in OLS and GLS methods, respectively, in Equations (8) and (9).

$$\Sigma_u = (P^T P)^{-1} P^T \Sigma_R P (P^T P)^{-1} \tag{8}$$

$$\Sigma_u = (P^T \Sigma_R^{-1} P)^{-1} \tag{9}$$

To determine confidence intervals for the parameter, the GUM suggests to use a Gaussian distribution (justified by the central limit theorem), and for other distributions to apply Monte Carlo simulations.

This approach is fully justified in cases of a lot of data having independent random uncertainties, but questionable for epistemic uncertainties that are often dependent and far from a Gaussian representation. And this approach generally leads to an over-optimistic assessment of uncertainties.

3.2 *Fuzzy approach*

Possibility theory was first introduced by Zadeh (1978). It is associated with the theory of fuzzy sets by the semantics of uncertainty that it gives the membership function. A possibility distribution $\pi(x)$ (Figure 2) is a mapping from a set to the unit interval such that $\pi(x) = 1$ for some x belonging to the set of reals. A possibility distribution π_1 is called more specific (i.e. thinner in a broad sense) than π_2 as soon as $\forall x \in \Re$, $\pi_1(x) \leq \pi_2(x)$ (fuzzy set inclusion). The more specific π is, the more informative it is. If for some x and $\pi(y) = 0$, for all $y \neq x$, then π is totally specific (fully precise and certain knowledge), if $\pi(x) = 1$ for all x then π is totally non-specific (complete ignorance).

In fact, a numerical degree of possibility can be viewed as an upper bound to a probability degree (Dubois *et al.* 2004). Namely, with every possibility distribution π one can associate a non-empty family of probability measures dominated by the possibility measure: $\mathcal{P}(\pi) = \{P, \forall A, P(A) \leq \Pi(A)\}$. This provides a bridge between probability and possibility, and there is also a bridge with interval calculus. Indeed, a unimodal numerical possibility distribution may also be viewed as a nested set of coverage intervals, which are the α-cuts of π: $[\underline{x}_\alpha, \overline{x}_\alpha] = \{x, \pi(x) \geq \alpha\}$. Obviously, the confidence intervals built around the same point x_0 are nested. It has been proven in Mauris *et al.* (2001) that stacking the coverage intervals of a probability distribution F on top of one another leads to a possibility distribution (denoted π^{x_0} having x_0 as modal value). In fact, in this way, the α-cuts of π^{x_0} are identified with the confidence interval $I^\star_\beta$ of probability level $\beta = 1 - \alpha$

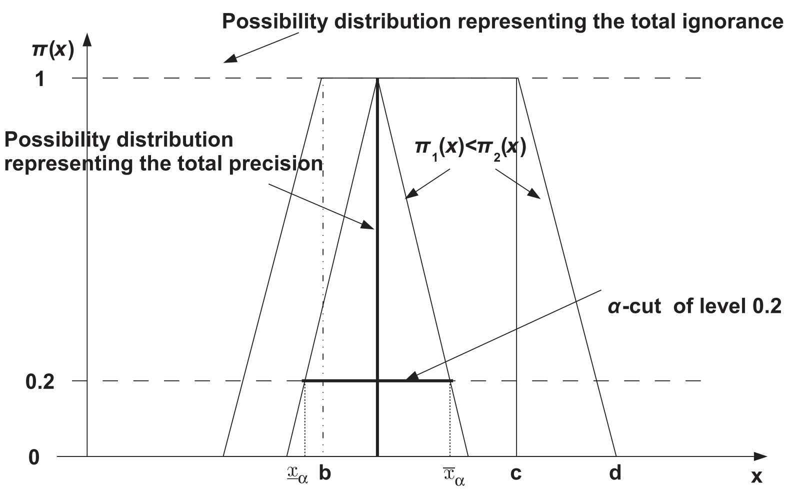

Figure 2. Example of fuzzy possibility distributions.

around the nominal value x_0. In this way a probability distribution can be represented by an equivalent possibility distribution. Moreover, a possibility distribution can be used for representing a family of probability distributions by taking the largest $1-\alpha$ confidence intervals obtained from each probability distribution of the family. This is useful to represent uncertainty when only partial probability knowledge is available. For example if the variable is known to be bounded and unimodal (with mode R) and with σ_R as standard deviation, then the maximum specific possibility distribution is a triangular possibility distribution with the mode R as vertex and with $[R-\sqrt{3}\sigma_R, R+\sqrt{3}\sigma_R]$ as support. In addition, due to the confidence interval interpretation, a possibility distribution is a convenient way to express expert knowledge. In summary, a possibility distribution can model both random and epistemic uncertainties in a unified modelling.

For the fuzzy approach, as no fully equivalent fuzzy least squares method is available, we use the GLS method to obtain the forward model (Equation (4)). Then we build the possibility distributions of the displacement from the nominal value R and their associated uncertainty σ_R, considering σ_R contains both random and epistemic components. Moreover, the measurements are considered as bounded (this is the case in the considered context), thus we represent them by a symmetric triangular fuzzy distribution with support $[R-\sqrt{3}\sigma_R, R+\sqrt{3}\sigma_R]$. Afterwards, the possibility distributions are propagated in the least squares adjustment using fuzzy arithmetic based on Zadeh's extension principle (Zadeh 1978, Bisserier *et al.* 2008):

$$u = (P^T \Sigma_R^{-1} P)^{-1} P^T \Sigma_R^{-1} \otimes R \tag{10}$$

where $\otimes$ denotes the fuzzy multiplication.

In this principle, the variables are considered as non-interactive variables; this corresponds somehow to considering a total dependence between variables. Consequently, uncertainty propagation by the fuzzy approach leads to an over-pessimistic assessment of uncertainties.

In order to perform comparisons of uncertainties between the conventional and the fuzzy approaches, it is necessary to represent the uncertainty in the fuzzy approach by a single parameter (similar to the variance in the conventional approach). The commonly used parameter is the full width at half maximum of the possibility distribution which corresponds to the width of the α-cut level of 0.5. Therefore, the full width at half maximum is $\sqrt{3}\sigma_R$. Let us note that with a Gaussian assumption of standard deviation σ_R, the value corresponding to the 0.5 α-cuts of the equivalent possibility distribution is equal to $1.35\sigma_R$.

3.3 *Uncertainty analysis by the two approaches*

In general, different modes of uncertainty representation and propagation in the conventional and the fuzzy approaches result in different behaviours of uncertainty evolution while adding more data sets in the linear inversion. With the conventional approach, Wright *et al.* (2004) have tested the effect of adding more data sets on the improvement of output uncertainty. The tests are performed by considering the same uncertainty for all of the input data sets. Here, we follow the same idea, and in addition to the tests in the conventional approach, we also perform the same tests in the proposed fuzzy approach. For this, four data sets with the same uncertainty are taken as input in the original inversion. Then we add one more data set each time in the inversion, and follow

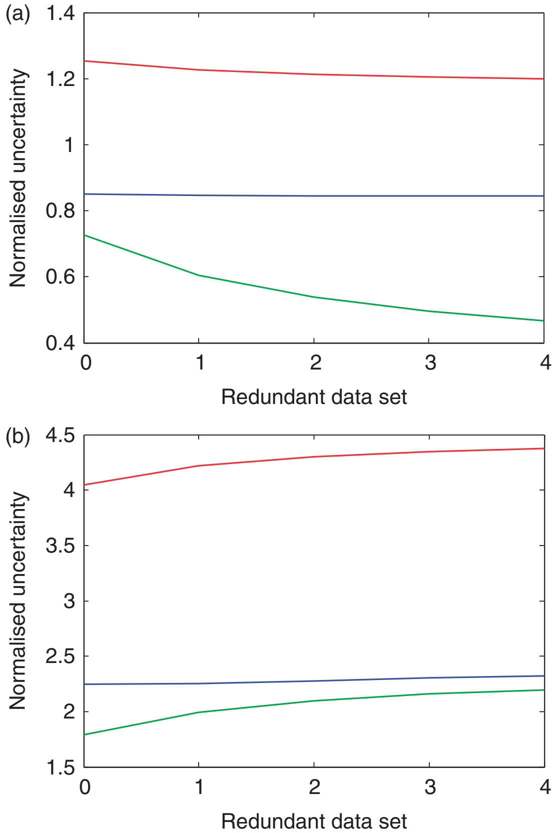

Figure 3. Evolution of the output uncertainty while adding more data sets in the inversion in (a) conventional and (b) fuzzy approaches. In this case, the dimension of the model vector u (see Equation (2)) is 3. P is a $4 \times 3, 5 \times 3, \ldots, 8 \times 3$ matrix that links the model and the data. Each colour curve in the figure corresponds to one component of the model vector, and the sensibility to the input data sets is different from one component to another. Uncertainties of all the input data sets are normalised to 1.

the evolution of the output uncertainty. Figure 3 is an example that illustrates the different behaviours of uncertainty in both approaches. First, the output uncertainties are always larger in the fuzzy approach than in the conventional approach. Second, the output uncertainties are reduced more or less significantly in the conventional approach, while they remain constant or even increase in the fuzzy approach. These observations are consistent with the different behaviours of both approaches mentioned in the previous Section.

3.4 *Model performance assessment*

In addition to the evaluation of the displacement uncertainties, geodesists often look for the difference between the model predictions and the data observations by computing residues. This practice aims at palliating for the lack of ground truth. Thus, the output model vector is projected into the space of data vector by the forward model, and then it is compared to the data vector.

In the conventional approach, the root mean square (RMS) is taken as index of evaluation. It can be calculated for each data set k as

$$RMS_k = \frac{\sum_{i=1}^{I_k} \frac{[R_k(i) - P_k(i) u_k(i)]^2}{\omega_k(i)}}{\sum_{i=1}^{I_k} \frac{1}{\omega_k(i)}} \tag{11}$$

where I_k is the number of pixel in each data set k, with

$$\omega = \begin{cases} 1, & \text{in OLS} \\ \sigma_R^2, & \text{in GLS} \end{cases}$$

A global residue over several data sets is derived as

$$RMS = \frac{\sum_{k=1}^{K} I_k RMS_k}{\sum_{k=1}^{K} I_k} \tag{12}$$

where K is the number of data set.

Note that in GLS, for each data set, the mean RMS_k is calculated by weighting each pixel by its corresponding coefficient in variance-covariance matrix, which is the same for inversion. For each scheme, the mean RMS is obtained by weighting the mean RMS_k of each data set by the number of pixels used in the inversion. A large value of RMS implies a large discrepancy between the modelled and the measured observations. In order to differentiate the contribution of pixels really used in the inversion from those not used (in pre-fusion, only a small number of pixels of good quality are used), three values of RMS are calculated: RMS_{used} is calculated on pixels really used in the inversion. It corresponds to the value minimised in the inversion. A small value of RMS_{used} implies a good coherence among data sets used in the inversion. $RMS_{\text{not-used}}$ is calculated on pixels not used in the inversion. And RMS_{total} is obtained taking into account all of the available pixels. In fact, RMS_{used} and RMS_{total} are two main criteria used for performance assessment.

For the fuzzy approach, each result u is obtained with a possibility distribution. The fuzzy model prediction $P \otimes u$ is computed by using fuzzy arithmetic. Then, instead of a comparison between two crisp values, a comparison between two possibility distributions (two symmetric triangular distributions) is performed in this article. In order to facilitate the comparison, the height of the triangle of intersection (h), which varies between 0 and 1, is taken as the index of evaluation (Figure 4). The more h is close to 1, the better is the agreement between the modelled and the measured observations.

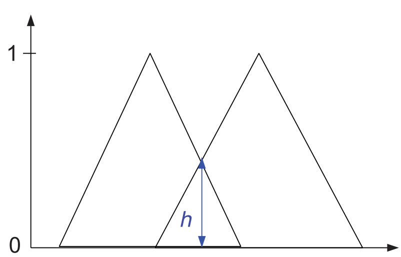

Figure 4. Illustration of intersection of two triangular distributions.

For each data set, the mean h_k is calculated by dividing the sum of h by the number of pixels.

$$h_k = \frac{\sum_{i=1}^{I_k} R_k(i) \wedge (P_k(i) \otimes u_k(i))}{I_k} \tag{13}$$

where $\wedge$ denotes the operator of intersection of two possibility distributions as illustrated in Figure 4.

A global fuzzy index over several data sets is obtainted as

$$h = \frac{\sum_{k=1}^{K} h_k I_k}{\sum_{k=1}^{K} I_k} \tag{14}$$

For each scheme, the mean h is calculated by weighting the mean h_k of each data set by the number of pixels used in the inversion. With the same objective as in the conventional approach, three values of h are computed: h_{used} is computed on pixels used in the inversion, $h_{\text{not-used}}$ is computed on pixels not used in the inversion, and h_{total} is obtained taking into account all of the available pixels.

4. Input data description

The sub-pixel image correlation and differential interferometry (D-InSAR) are two conventional techniques used to extract displacement measurements from SAR data. The sub-pixel image correlation calculates the offsets in range (line of sight) and azimuth (along the satellite trajectory) directions on amplitude images, with a sub-pixel accuracy. It is widely used to measure displacements of large magnitudes (Pathier *et al.* 2006, Wright *et al.* 2006, Yun *et al.* 2007). Based on the phase information, D-InSAR can measure the displacement in range direction with an accuracy of the order of cm, or mm (Carnec and Raucoules 2000, Carnec *et al.* 2000). This technique is usually applied to measure displacements of small magnitude. In the case of a strong earthquake induced by a rupture of a fault, in the near field of the fault, the measurements from sub-pixel image correlation can provide reliable displacement information (Pathier *et al.* 2006). While in the far field of the fault, the measurements from D-InSAR are taken as precise sources.

In this article, a series of coseismic ENVISAT images, acquired for both ascending[1] and descending[2] modes, from October 2004 to June 2006, is used to estimate the deformation due to the 2005 Kashmir earthquake. Twenty two measurements from sub-pixel image correlation and five measurements from D-InSAR, are obtained. The availability of different types of measurements is shown in Figure 5. Figure 6 illustrates these two types of measurements with their associated uncertainties. In the near field of the fault, because of coherence loss, phase information cannot be extracted by D-InSAR, thus there are no D-InSAR measurements available in this area. These measurements can be classified in four families according to their acquisition geometry: ascending range (Asc. Rg), ascending azimuth (Asc. Az), descending range (Des. Rg) and descending azimuth (Des. Az). In each family, in a first approximation, all the measurements are considered to correspond to the same displacement (in the same direction), since the incident angle is the same for all the measurements.

Figure 7 illustrates the uncertainty present in the measurements from both sub-pixel image correlation and D-InSAR by plotting two profiles from the displacement images shown in Figure 6. Profile (1) is located in an area far from the fault and Profile (2) passes

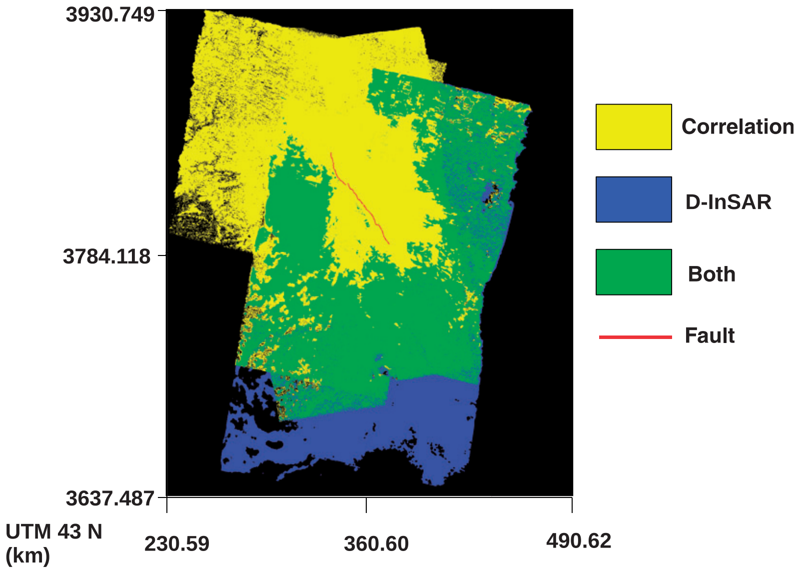

Figure 5. Availability of different types of measurements.

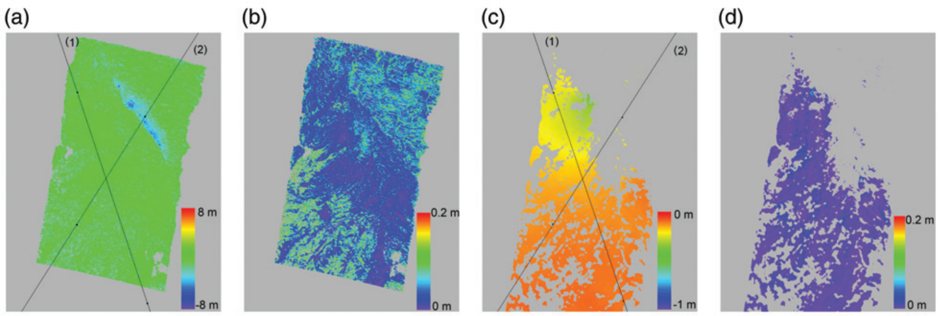

Figure 6. Displacement and associated uncertainty in range direction estimated by sub-pixel image correlation (a), (b) and D-InSAR (c), (d). Profiles (1) and (2) are used for uncertainty analysis thereafter.

across the fault. In theory, the same displacement values should be found by these two techniques where both measurements are available, as they measure exactly the same quantity of displacement. However, with the presence of uncertainty in both measurements, a discrepancy of displacement values is observed on both profiles. On one hand, a significant fluctuation of displacement value is observed in the sub-pixel image correlation measurements, which implies the presence of random uncertainty. Near the fault, the fluctuation is small, while in the area far from the fault where the displacement magnitude is small, the fluctuation becomes significant. On the other hand, there is a small shift between the displacement values estimated by both techniques. Consequently, it is probable that epistemic uncertainty is present in one or the other measurement. However, it seems that the random uncertainty is more important than the epistemic uncertainty in our data sets.

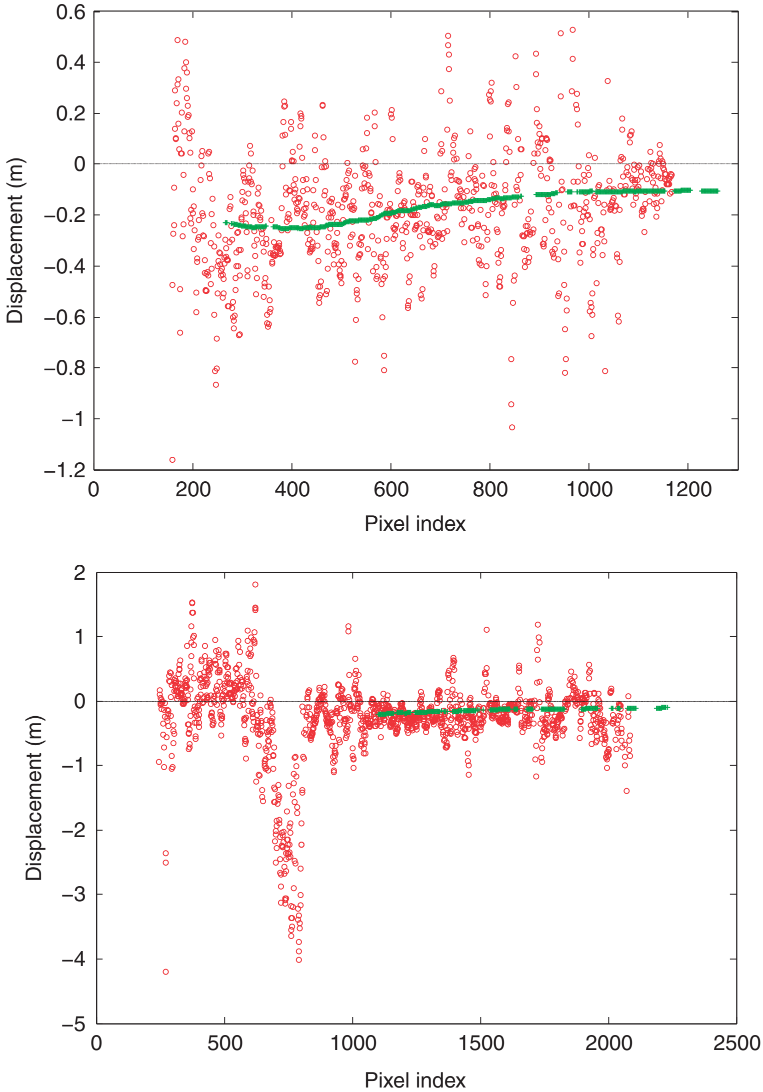

Figure 7. Illustration of uncertainties present in measurements from both sub-pixel image correlation (red dots) and D-InSAR (green lines). Descending Track 463 (2004/11/06 – 2005/11/26) (a) on Profile (1) and (b) on Profile (2) reported on Figure 6.

For measurements from sub-pixel image correlation (denoted by Cor. thereafter), the uncertainty is represented by the pseudo-variance associated with the displacement value obtained from the correlation technique in ROIPAC software (Rosen *et al.* 2004), which implies the quality of cross-correlation between two amplitude images. Random uncertainty exists in these measurements because of decorrelation noise present in the data. However, epistemic uncertainty can be present due to the DEM errors or defects in the correlation method, which is difficult to quantify. As a result, the pseudo-variance used as uncertainty is considered to include both random and epistemic components. Note that the possible epistemic uncertainty due to the imperfect data processing is not included in the pseudo-variance. For measurements from D-InSAR (denoted by ϕ thereafter), the uncertainty corresponds to the variance of the phase value estimated from the filtered coherence (Trouvé *et al.* 1998). It characterises essentially random variations in phase values. However, epistemic uncertainty due to, for example, phase unwrapping errors, atmospheric impacts, is probably present in the measurements, and it should be taken into account in the fusion schemes and uncertainty management approaches.

5. Retrieval of 3D displacement field and associated uncertainty at the Earth's surface

5.1 *Problem statement and method*

Different measurements from sub-pixel image correlation and D-InSAR are different projections in the range and azimuth directions of the 3D displacement field at the Earth's surface (E, N, Up)[3] (Figure 8). Consequently, the 3D displacement field can be constructed from at least three different projections by a linear inversion. In this case, in Equation (2), R corresponds to the different measurements from sub-pixel image correlation and D-InSAR and the matrix P corresponds to the projection vectors matrix. u denotes the 3D displacement field with three components E, N, Up.

To solve this linear inverse problem, the least squares methods (OLS and GLS) are used. The uncertainties are represented by the conventional approach and a fuzzy approach. Two fusion schemes: pre-fusion and joint inversion are investigated. In pre-fusion, the data set with the smallest uncertainty among all of the available data sets is selected in each family. Then, the inversion is realised with four selected data sets on

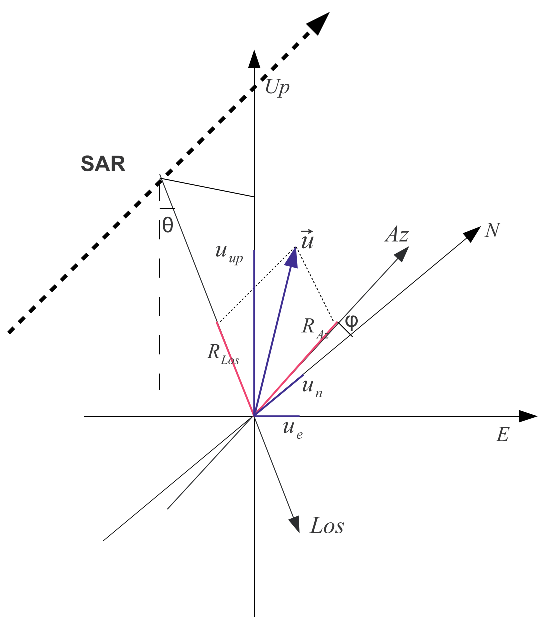

Figure 8. 3D (E, N, Up) displacement field and SAR acquisition geometry (range/azimuth directions) for ascending pass. u denotes a 3D vector with 3 components u_e, u_n and u_{up}. R_{Los} and R_{Az} represent the projections of u in range and azimuth direction respectively. θ is the incident angle. φ corresponds to the angle between the North and the Azimuth direction.

each pixel. In joint inversion, the inversion is performed using all of the available data sets on each pixel. Note that, due to the geographic position of different data sets, the number of available data sets can be different from one pixel to another. The results are shown in Figure 9, and analysed in the following section.

5.2 *Comparison of results*

In order to highlight the advantages and disadvantages of each fusion scheme and uncertainty management approach, three levels of comparisons are performed: between displacement values, between uncertainties and between fuzzy distributions. In addition, the effect of uncertainty reduction due to adding D-InSAR measurements is analysed. For this, four different cases are defined:

(1) Pre-fusion on the data sets from sub-pixel image correlation.
(2) Pre-fusion on the data sets from both sub-pixel image correlation and D-InSAR.
(3) Joint inversion on the data sets from sub-pixel image correlation.
(4) Joint inversion on the data sets from both sub-pixel image correlation and D-InSAR.

Regarding the displacement value (Figure 9(a)), the results in different cases are globally consistent, with an average difference in the order of mm and an RMS included between 10 cm and 25 cm. Table 1 shows the displacement value differences of the Up component between the different cases studied in this article and the results found by Pathier *et al.* (2006) by using three measurements from sub-pixel image correlation. The difference with respect to results found by Pathier *et al.* is larger, which can be explained by the uncertainty associated with measurements and by the extra data sets used in this article. As there is no ground truth available, in order to evaluate in detail each fusion scheme and uncertainty management approach, the residues are calculated.

The results obtained by using the conventional approach are shown in Tables 2 and 3. First, the RMS_{used} and RMS_{total} are smaller in GLS than in OLS. This is consistent with the fact that in GLS, the contribution of the data sets whose uncertainty is large is less important. Thus, the weighting of different data sets, more or less reliable, is important. Second, between pre-fusion and joint inversion, the RMS_{total} in joint inversion is slightly smaller than in pre-fusion, as joint inversion reduces mostly the random uncertainty. However, the RMS_{used} in pre-fusion is much smaller, which can be explained by the good quality of the data sets used and the reduced number of data sets used in the inversion: there are four data sets in the inversion with pre-fusion, and they are compatible to each other, thus it is easier to find a model fitting these data. Finally, the benefit of adding data sets from D-InSAR, in both pre-fusion and joint inversion schemes is a reduction in the RMS_{used} and RMS_{total}.

The pseudo-residues in the fuzzy approach, given by Equation (14), are shown in Table 4. The values of h_{used} and h_{total} in pre-fusion are larger than those in joint inversion. The pre-fusion is thus preferred for the fuzzy approach. With the addition of data sets from D-InSAR, the values of h_{used} and h_{total} decrease. This behaviour indicates that epistemic uncertainty probably exists in our data sets and that it has been taken into account by the fuzzy approach.

Regarding the uncertainty value, the evolution of uncertainty varies from one case to another. In the conventional approach, the uncertainties are smaller in joint inversion than

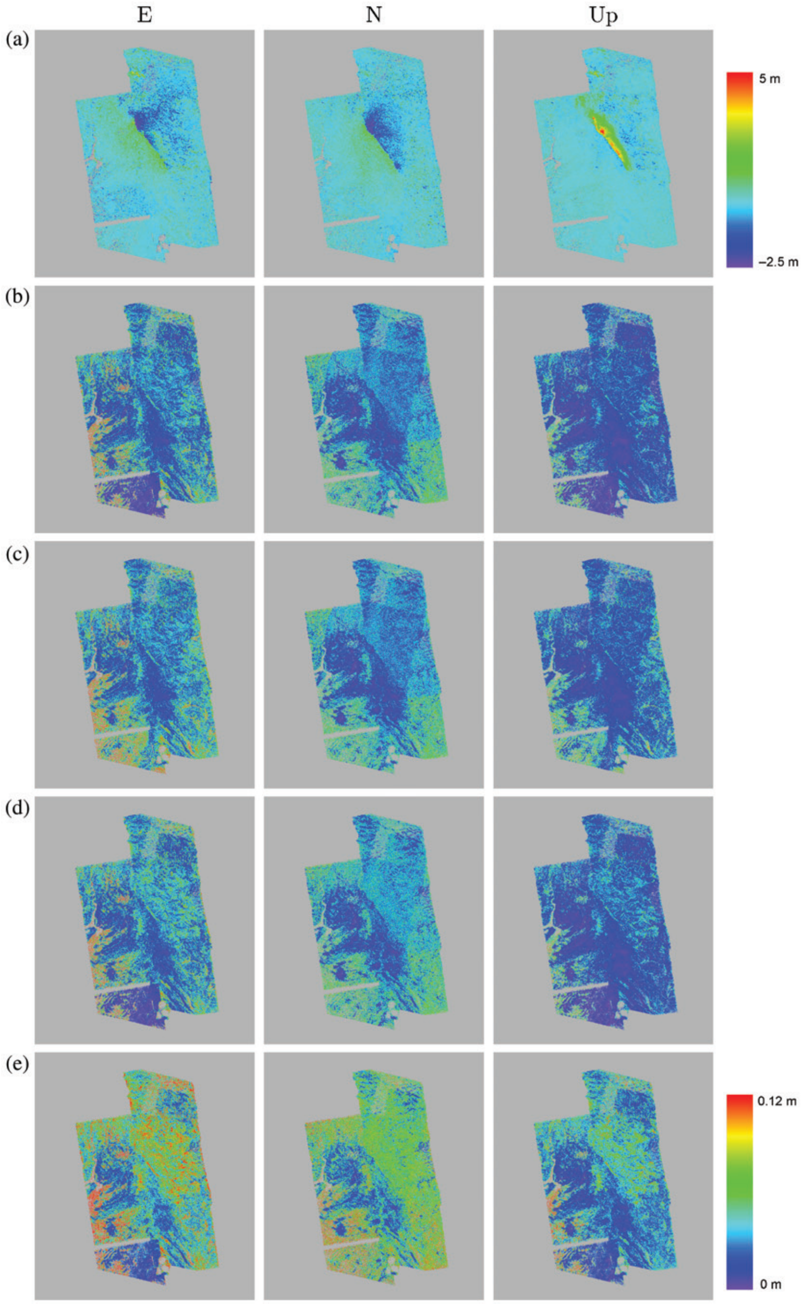

Figure 9. 3D displacement field: (a) displacement value (b)–(e) associated uncertainty; (a), (b) joint inversion with D-InSAR data sets in the conventional approach; (c) joint inversion without D-InSAR data sets in the conventional approach; (d) pre-fusion with D-InSAR data sets in the conventional approach and (e) joint inversion with D-InSAR data sets in the fuzzy approach.

Table 1. Difference of Up component displacement value between different cases studied in this article and the results found by Pathier *et al*. (2006). GLS method.

–	Pre-fusion, Cor.		Pre-fusion, Cor., ϕ		Joint inversion, Cor.		Joint inversion, Cor., ϕ		Pathier *et al.*	
–	Mean (m)	RMS (m)	Mean (m)	RMS (m)	Mean (m)	RMS (m)	Mean (m)	RMS (m)	Mean (m)	RMS (m)
Pre-fusion, Cor.	0	0	−0.0013	0.1895	0.0053	0.1699	0.0080	0.2340	0.0920	0.6385
Pre-fusion, Cor., ϕ	−0.0013	0.1895	0	0	0.0040	0.2291	0.0066	0.1637	0.0852	0.6209
Joint inversion, Cor.	0.0053	0.1699	0.0040	0.2291	0	0	−0.0026	0.1522	0.0855	0.5954
Joint inversion, Cor., ϕ	0.0080	0.2340	0.0066	0.1637	−0.0026	0.1522	0	0	0.0804	0.5831
Pathier *et al.*	0.0920	0.6385	0.0852	0.6209	0.0855	0.5954	0.0804	0.5831	0	0

Table 2. RMS of displacement value in different fusion schemes using different types of measurements for OLS method. See corresponding text for details.

	Joint inversion		Pre-fusion	
OLS	Cor.	Cor., ϕ	Cor.	Cor., ϕ
RMS_{used} (m)	0.5468	0.4900	0.3148	0.3120
$RMS_{\text{not-used}}$ (m)	–	–	0.7835	0.6605
RMS_{total} (m)	0.5468	0.4900	0.6402	0.5708

Table 3. RMS of displacement value in different fusion schemes using different types of measurements for GLS method. See corresponding text for details.

	Joint inversion		Pre-fusion	
GLS	Cor.	Cor., ϕ	Cor.	Cor., ϕ
RMS_{used} (m)	0.1156	0.1133	0.0281	0.0266
$RMS_{\text{not-used}}$ (m)	–	–	0.2528	0.2301
RMS_{total} (m)	0.1156	0.1133	0.1337	0.1292

Table 4. Height of triangle of intersection in different fusion schemes using different types of measurements. See corresponding text for details.

	Joint inversion		Pre-fusion	
Fuzzy	Cor.	Cor., ϕ	Cor.	Cor., ϕ
h_{used} (m)	0.3170	0.2830	0.5640	0.5294
$h_{\text{not-used}}$ (m)	–	–	0.1677	0.1445
h_{total} (m)	0.3170	0.2830	0.3653	0.3405

in pre-fusion (Figure 9(b) (joint inversion) and (d) (pre-fusion)) because of the contribution of a large number of data sets used in joint inversion. On the contrary, in the fuzzy approach, the uncertainties are smaller in pre-fusion than in joint inversion, which is consistent with the general behaviour of this approach. Adding data sets from D-InSAR reduces the uncertainties in both conventional and fuzzy approaches. Figure 9(b) and (c) illustrates this effect in the conventional approach. In the far field of the fault, where data sets from D-InSAR are available, the uncertainties are reduced (Figure 9(b) with D-InSAR data sets with respect to Figure 9(c) without D-InSAR data sets), especially in the Up component. Finally, the uncertainties in the fuzzy approach are always larger than those in the conventional approach, as shown in Figure 9(b) (conventional approach) and (e) (fuzzy approach), which is coherent with the synthetic tests in Section 3.3.

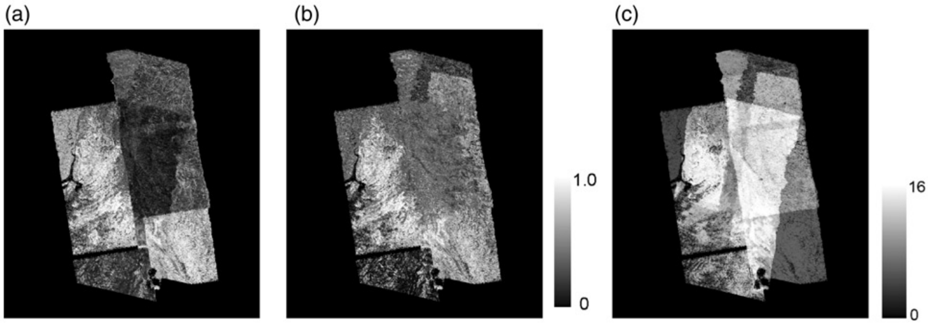

Figure 10. (a), (b) Ratio of conventional uncertainty to fuzzy uncertainty, with D-InSAR data sets, E component in joint inversion and pre-fusion, respectively. (c) Number of available data sets for 3D displacement retrieval.

In order to understand the spatial evolution of uncertainty in both approaches, the ratio of conventional uncertainty to fuzzy uncertainty is performed. In joint inversion, a geographic effect is observed (Figure 10(a)). It corresponds to the distribution of the number of available data sets (Figure 10(c)). In the darker area, the difference between two uncertainties is large, because in this area there are more data sets available. In the conventional approach, the output uncertainty is reduced. In the fuzzy approach, on the contrary, the output uncertainty remains constant or increases slightly. Consequently, the difference between two uncertainties increases. In pre-fusion, the ratio is relatively homogeneous. As there are only four data sets in the inversion, the effect due to the different ways of uncertainty propagation is less visible. However, the effect due to the addition of D-InSAR measurements is observed (Figure 10(b)). In the areas where D-InSAR measurements are available (Figure 5), as their uncertainties are much smaller than those of sub-pixel image correlation measuresment, in both approaches, the output uncertainty is reduced. This results in a less significant difference between uncertainties in both approaches.

5.3 *Discussion*

These results show that the conventional approach and the fuzzy approach behave differently with the different fusion schemes: the conventional approach is adapted to joint inversion while the fuzzy approach favors the pre-fusion. Consequently, the choice of fusion scheme depends on the nature of the uncertainty, how to represent and propagate the uncertainty, and the user's knowledge of the information sources.

Regarding the conventional approach, with respect to the reduction of random uncertainty, in most cases, joint inversion is robust. However, in certain cases, joint inversion and pre-fusion give the same results. For instance, when the same measurements from both sub-pixel image correlation and D-InSAR are available, the uncertainty of sub-pixel image correlation measurements is usually much larger than that of D-InSAR measurements. On one hand, for joint inversion with the GLS method, the contribution from the sub-pixel image correlation measurements is negligible with respect to the contribution from D-InSAR measurements. On the other hand, in pre-fusion, only the D-InSAR measurements are selected in the inversion. Therefore, joint inversion and pre-fusion give almost the same results. In this case, pre-fusion is preferable, because it is less time consuming. Finally, adding measurements from D-InSAR reduces uncertainty due to their great accuracy, in particular in the far field of the fault where the measurements of sub-pixel image correlation become less reliable.

The fuzzy approach can be considered as an interesting and intuitive alternative for representing measurement uncertainty. The fuzzy approach is free from the assumptions of Gaussian distribution and independence. The output uncertainty is more pessimistic than for the conventional approach, but more robust when these assumptions are not valid. In addition, the evolution of uncertainty with different schemes is different from that in the conventional approach: the output uncertainty is smaller in pre-fusion compared to that in joint inversion.

6. Conclusions and perspectives

In this article, two fusion schemes, pre-fusion and joint inversion, are investigated in a linear inversion problem for displacement measurement in geophysics. Two approaches of uncertainty management, the conventional approach and the fuzzy approach, based on probability and possibility theory, respectively, are applied. The experimental results are presented with application to the retrieval of 3D displacement fields at the Earth's surface due to the 2005 Kashmir earthquake. The advantages and disadvantages of each fusion scheme or uncertainty management approach are highlighted by comparisons.

For the conventional approach, adding more data sets leads to a reduction of uncertainty, which is why joint inversion with the GLS method is the favoured process for most geophysicists. However, this approach is realised assuming that the uncertainty associated with each data set is random. In most cases, in order to facilitate the processing, the independence is also assumed. The fuzzy approach is free from these hypotheses. It provides a different view of uncertainty management and takes into account the epistemic uncertainty, which favors the scheme of pre-fusion. With the considered data sets, the uncertainty obtained in the conventional approach is considered as too optimistic, while the uncertainty obtained in the fuzzy approach is too pessimistic. As a result, the actual uncertainty should be situated between these two uncertainties.

In this article, the fuzzy approach has been investigated by modelling the uncertainty only with a symmetric triangular distribution; the richness and the flexibility of different fuzzy distributions have not yet been exploited. For post-fusion, because of the geographic positions of the data sets, it is difficult to implement this scheme with the available data sets over large area. However, the combination of SAR measurements and optical measurements by post-fusion will be performed in the future. Furthermore, the application of fusion schemes and uncertainty management approaches to the estimation of fault parameters by nonlinear inversion of a mechanical deformation model constitutes an interesting perspective.

Acknowledgements

This work was supported by the EFIDIR project (http://www.efidir.fr; No. ANR-07-MDCO-004) and the PAKSIS program CATTELL, granted by the French National Agency (ANR). The authors thank the ANR for their support. The ENVISAT data sets are available thanks to ESA project category 1, No. 3802. The authors also thank the reviewers for their help in improving the manuscript.

Notes

1. IS6, swath positionning of sensor with a nominal incidence angle of $\sim 42^{\circ}$.
2. IS2, swath positionning of sensor with a nominal incidence angle of $\sim 23^{\circ}$.
3. (E, N, Up) is also known as Local Tangent Plane. It is a geographical coordinate system for representing state vectors that is commonly used in aviation. It consists of three numbers, one represents the position along the eastern axis, one along the northern axis and one represents vertical position.

References

Attema, E., 2005. Mission requirements document for the European radar observatory sentinel-1. *ES-RS-ESA-SY-0007*, Issue 1.

BIPM, IEC, IFCC, ILAC, ISO, IUPAC, IUPAP, and OIML, 2008. *Evaluation of measurement data – guide to the expression of uncertainty in measurement*. Geneva: JCGM 2008 edition.

Bisserier, A., Boukezzoula, R., and Galichet, S., 2008. Linear fuzzy regression using trapezoidal fuzzy intervals. *In*: *12th International Conference on Information Processing and Management of Uncertainty in Knowledge Based Systems (IPMU 2008)*. Malaga, Spain, 181–188.

Carnec, C. and Raucoules, D., 2000. Assessement of SAR interferometry within operational application: mapping and modelling of peri-urban subsidence. *In*: *ESA-ENVISAT Symposium*. Gothenburg, Sweden, 5.

Carnec, C., *et al.*, 2000. Mapping and modelling of major urban subsidence on Mexico City from radar interferometry. *In*: *International Conference the Fragile Territory*. Rome, Italy, 25–28.

Cervelli, P., Murray, M.H., and Segall, P., 2001. Estimating source parameters from deformation data, with an application to the March 1997 earthquake swarm off the Izu Peninsula, Japan. *Journal of Geophysical Research*, 106 (B6), 11217–11237.

Cornillon, P. and Matzner-Lober, E., 2007. *Régression, théorie et applications*. Paris: Springer.

Davidson, R. and Mackinnon, J.G., 1993. *Estimation and inference in econometrics*. 9th ed. Oxford: Oxford University Press.

Doin, M., *et al.*, 2009. Corrections of stratified tropospheric delays in SAR interferometry: validation with global atmospheric models. *Journal of Applied Geophysics*, 69 (1), 35–50.

Dubois, D., *et al.*, 2004. Probability-possibility transformations, triangular fuzzy sets and probabilistic inequalities. *International Journal on Reliable Computing*, 10 (4), 273–297.

Dubois, D. and Prade, H., 1988. *Possibility theory: an approach to computerized processing of uncertainty*. New York: Plenum Press.

Grandin, R., *et al.*, 2009. September 2005 Manda Hararo–Dabbahu rifting event, Afar (Ethiopia): constraints provided by geodetic data. *Journal of Geophysical Research*, 114 (B08404), B08404.1–B08404.20.

Jacquin, A., 2010. Possibilistic uncertainty analysis of a conceptual model of snowmelt runoff. *Hydrology and Earth System Sciences*, 14, 1681–1695.

Lohman, R.B. and Simons, M., 2005. Some thoughts on the use of InSAR data to constrain models of surface deformation: noise structure and data downsampling. *Geochemistry, Geophysics, Geosystems*, 6 (1), Q01007.1–Q01007.12.

Lu, Z., *et al.*, 2010. Radar image and data fusion for natural hazards characterisation. *International Journal of Image and Data Fusion*, 1 (3), 217–242.

Mauris, G., Lasserre, V., and Foulloy, L., 2001. A fuzzy approach for the expression of uncertainty in measurement. *International Journal of Measurement*, 29 (3), 165–177.

Mujumdar, P. and Ghosh, S., 2008. Modeling GCM and scenario uncertainty using a possibilistic approach: application to the Mahanadi River, India. *Water Resources Research*, 44 (W06407), W06407.1–W06407.15.

Pathier, E., *et al.*, 2006. Displacement field and slip distribution of the 2005 Kashmir earthquake from SAR imagery. *Geophysical Research Letters*, 33 (L20310), L20310.1–L20310.5.

Pedersen, R., *et al.*, 2003. Fault slip distribution of two June 2000 M_w6.5 earthquake in South Iceland estimated from joint inversion of InSAR and GPS measurements. *Earth and Planetary Science Letters*, 213, 487–502.

Rao, C., 1973. *Linear statistical inference and its applications*. 2nd ed. New York: John Wiley & Sons.

Rosen, P., *et al.*, 2004. Updated repeat orbit interferometry package released. *Transactions, American Geophysical Union*, 85 (47), 47.

Ross, J., Ozbek, M., and Pinder, G., 2009. Aleatoric and epistemic uncertainty in groundwater flow and transport simulation. *Water Resources Research*, 45 (W00B15), W00B15.1–W00B15.10.

Schmidt, D.A., *et al.*, 2005. Distribution of aseismic slip rate on the hayward fault inferred from seismic and geodetic data. *Journal of Geophysical Research*, 110 (B08406), B08406.1–B08406.15.

Shafer, G., 1976. *A mathematical theory of evidence*. Princeton: Princeton University Press.

Sudhaus, H. and Jónsson, S., 2009. Improved source modelling through combined use of InSAR and GPS under consideration of correlated data errors: application to the June 2000 Kleifarvatn earthquake, Iceland. *Geophysical Journal International*, 176 (2), 389–404.

Tarantola, A., 2005. *In*: A. Tarantola, ed. *Inverse problem theory and methods for model parameter estimation*. Philadelphia: Society for Industrial and Applied Mathematics edition, 57–80.

Tarantola, A. and Valette, B., 1982. Generalized nonlinear inverse problems solved using the least squares criterion. *Review of Geophysics and Space Physics*, 20 (2), 219–232.

Trouvé, E., Nicolas, J., and Maitre, H., 1998. Improving phase unwrapping techniques by the use of local frequency estimates. *IEEE Transaction on Geoscience and Remote Sensing*, 36 (6), 1963–1972.

Verhoest, N., *et al.*, 2007a. A possibilistic approach to soil moisture retrieval from ERS synthetic aperture radar backscattering under soil roughness uncertainty. *Water Resources Research*, 43 (W07435), W07435.1–W07435.13.

Verhoest, N., Baets, B.D., and Vernieuwe, H., 2007b. A Takagi–Sugeno fuzzy rule-based model for soil moisture retrieval from SAR under soil roughness uncertainty. *IEEE Transaction on Geoscience and Remote Sensing*, 45 (5), 1351–1360.

Wright, T.J., *et al.*, 2006. Magma-maintained rift segmentation at continental rupture in the 2005 Afar dyking episode. *Nature*, 442, 291–294.

Wright, T.J., Parsons, B.E., and Lu, Z., 2004. Toward mapping surface deformation in three dimensions using InSAR. *Geophysical Research Letters*, 31 (L01607), L01607.1–L01607.5.

Yun, S.H., *et al.*, 2007. Interferogram formation in the presence of complex and large deformation. *Geophysical Research Letters*, 34 (L12305), L12305.1–L12305.6.

Zadeh, L.A., 1978. Fuzzy sets as a basis for a theory of possibility. *Fuzzy Sets and Systems*, 1 (1), 3–28.